Iranian Journal of Science and Technology, Transactions of Electrical Engineering (2022) 46:1149–1174
https://doi.org/10.1007/s40998-022-00524-2

RESEARCH PAPER

Optimal Sizing of Hybrid Renewable Energy System for Electricity Production for Remote Areas

Priyanka Anand[1] · Mohammad Rizwan[2] · Sarbjeet Kaur Bath[3] · Gulnar Perveen[4] · Vikram Kumar Kamboj[5,6]

Received: 23 July 2020 / Accepted: 11 June 2022 / Published online: 25 July 2022

Abstract
Today, the world is looking at the adoption of alternative energy resources for electrical power generation, particularly for remote applications. Renewable energy resources are being investigated to meet such demand due to numerous benefits, such as being environmentally friendly, a reliable source of energy, improving public health issues, job creation in rural areas, and so on. In the present work, two intelligent approaches, including a recently developed method named Improved Harmony Search (IHS) and Particle Swarm Optimization (PSO), have been adopted for the optimal sizing of the hybrid renewable energy system to fulfill the electrical load demand of a selected remote site in the Haryana state of India. The problem has been formulated by developing a mathematical model of the hybrid renewable energy system by considering the capital cost, replacement cost, operation and maintenance (O & M) cost, fuel cost, salvage value of various components, and the cost of selling and buying power to and from the utility grid. The optimization of the hybrid model for off-grid and grid-connected mode has been carried out for the minimization of the Net Present Cost (NPC) of the hybrid system by using the MATLAB platform. A comparative analysis of the results obtained by using the IHS and PSO algorithms is also presented in this work.

Keywords Renewable energy resources · Solar energy · Solar photovoltaic · Intelligent approach · Hybrid energy system

1 Introduction

Electricity is very important for improving the living standards of people and for a country's economic growth. The majority of the population living in developing nations belongs to rural communities. A large chunk of this rural population relies entirely on biomass or fossil fuels to cook food or to satisfy other needs for energy, but the burning of fossil fuels pollutes the atmosphere and creates greenhouse gas (GHG) emissions that cause global warming and are not good for human health (Chauhan and Saini 2015; Dey et al. 2019; Lu and Wang 2020). In addition to that, the regular supply of electricity to most rural areas is limited to a few hours, for many reasons, such as an inadequate distribution system, energy theft, the reluctance of local people to pay electricity bills, etc. These issues can be resolved by utilizing locally available renewable energy resources for distributed power generation. It is also observed that the whole world is looking to increase the contribution of renewable energy resources to make the power sector more reliable and more efficient. Further, the

✉ Priyanka Anand
anand_priyanka10@yahoo.co.in

1 Department of Electronics and Communication Engineering, B.P.S. Mahila Vishwavidyalaya, Sonipat, Haryana 131305, India

2 Department of Electrical Engineering, Delhi Technological University, Delhi 110042, India

3 Department of Electrical Engineering, Giani Zail Singh Campus College of Engineering and Technology, Bathinda, Punjab 151001, India

4 Defence Research and Development Organisation, Metcalfe House Annexe, Delhi, India

5 School of Electronics and Electrical Engineering, Lovely Professional University, Phagwara, Punjab, India

6 Schulich School of Engineering, University of Calgary, Calgary, AB, Canada

Ministry of New and Renewable Energy (MNRE), India, has an ambitious target of 175 GW by the end of 2022 (MNRE 2020). It is common knowledge that most renewable energy resources fluctuate in nature, necessitating additional backup for energy storage systems. If battery energy storage is utilized as a backup, it will enhance the cost of the system and the cost of energy (CoE) as well. To overcome these issues, a hybrid energy system (HES) can be developed by utilizing all the locally available renewable energy resources.

Many researchers have employed extensive methodologies such as simulation (Anand et al. 2017), graphical construction (Borowy and Salameh 1996; Markvart 2006), probabilistic (Karaki et al. 1999; Lujano et al. 2013), iterative (Li et al. 2012; Zhang et al. 2013), artificial intelligence (Alturki et al. 2020; Askarzadeh 2013b, a; Alaaeldin et al. 2018; Chauhan and Saini 2017; Delnia et al. 2020; Mubaarak et al. 2021; Paliwal et al. 2014; Li et al. 2020; Wu et al. 2020; Das and Hasan 2021), etc. to address critical issues related to the optimum design and sizing of the equipment used in a HES. Moreover, several authors applied intelligent approaches like Genetic Algorithm (GA), Particle Swarm Optimization (PSO), Harmony Search (HS), Ant Colony Optimization (ACO), Biogeography-Based Optimization (BBO), and Grey Wolf Optimization (GWO) to optimize HES_s to maximize economic benefits.

Delnia et al. carried out research for optimal sizing of micro-grid based on solar photovoltaic (SPV)/Wind/Battery and SPV/Wind/Battery/Electric Vehicle, by using PSO and the SPV/Wind/Battery system was found to be more economical (Delnia et al. 2020). Arévaloa et al. investigated five types of storage batteries for hybrid systems such as lead-acid, lithium-ion, vanadium redox flow, and hydrogen, hydrogen-vanadium redox flow were analyzed using HOMER (Hybrid Optimization of Multiple Energy Resources) software, and the vanadium redox flow battery was revealed to be the most effective in terms of net present cost (NPC) and cost of energy (CoE) (Arévaloa et al. 2020). Li et al. proposed a model based on universal size optimization for the hybrid SPV-wind-battery system using the PSO algorithm to determine the optimal configuration of a water pumping system. The developed model was able to meet the power requirements of the system (Li et al. 2020). Alaaeldin et al. proposed an efficient grid-integrated SPV/Wind hybrid system using the hybrid PSO-GWO method for operating a desalination plant for reverse osmosis. In this research, systems such as SPV/Wind/battery and SPV/Wind/Hydrogen storage have been compared in terms of both cost minimization and CO_2 emissions. The results demonstrate that the SPV/Wind along with the battery storage system is more economical and environmentally friendly (Alaaeldin et al. 2018).

The study of the optimal sizing of renewable HES_s by Bartolucci et al. revealed two findings. Firstly, the fuel cell (FC) system affects the stability of the grid, and secondly, the correct size of the SPV power plant allows the battery to be used more intelligently and gives less reliance on the energy exchanged with the grid (Bartolucci et al. 2018). Chauhan and Saini have proposed a Discrete Harmony Search (DHS)-based approach to optimize the size of a hybrid power system to reduce NPC (Chauhan and Saini 2016). The technique of HS optimization to size a grid-dependent SPV-based system for homes located in Iran was also applied by Zebarjadi and Askarzadeh. The results conclude that the SPV system is more economical in circumstances wherein the price of electricity rises from the current perception (Zebarjadi and Askarzadeh 2016). Singh et al. proposed an ABC algorithm for optimum sizing of a hybrid system for electricity generation in the rural areas of Punjab state in India. The results obtained were found to be more economical as compared to PSO and HOMER (Singh et al. 2016). Eteiba et al. conducted a techno-economic analysis of an off-grid hybrid system consisting of SPV/biomass/battery for meeting Egypt's electricity demand. In the research, three types of batteries, namely flooded lead-acid, Nickel Iron, and Lithium Ferro Phosphate, were considered, and optimal sizing has been done using four optimization techniques, viz. the Flower Pollination Algorithm (FPA), ABC, HS, and the Firefly Algorithm (FA). FA provides more accurate results with minimum execution time (Eteiba et al. 2018). The FA was also employed by Sufyan et al. for economic scheduling and optimization of the battery capacity of an isolated micro-grid. The results were also compared with those obtained by applying ABC, HS, and PSO, and a 50% decline in operating cost was obtained with the use of the proposed FA algorithm (Sufyan et al. 2019).

Anand et al. exploited the PSO algorithm for the optimal design and sizing of the SPV/biomass/biogas and battery-based hybrid system for rural electrification, which includes eight different models. The finding indicates that the configuration comprising of SPV/biogas/biomass performed better than other configurations (Anand et al. 2019a). The same authors attempted to optimize the size of a grid-integrated hybrid SPV/biogas/biomass/battery system for meeting the demand for electricity in Haryana (India).Various configurations are considered and contrasted by employing the GWO algorithm in both off-grid and grid-connected scenarios. It has been concluded from the results that the configuration connected to the grid was found to be the best configuration for the selected area (Anand et al. 2019b). The same authors also carried out the optimal design of a hybrid system consisting of renewable energy resources using two configurations, i.e., hybrid grid-integrated and off-grid systems using the HS algorithm. It has been revealed from the results that a grid-integrated hybrid system comprising SPV/Wind/ biogas/biomass with a battery is the most economical (Anand et al. 2020). Ghaffari and Askarzadeh proposed a modified Crow Search Algorithm (CSA) for the optimal design of hybrid SPV/DG/FC for the minimization of total NPC. It is concluded from the research that the proposed model gave more accurate results when compared with the original CSA, PSO, and GA (Ghaffari and Askarzadeh 2020). Wu et al. used the Salp Swarm Algorithm (SSA) to optimize the size of a grid-connected HES associated with a pumped-storage system. Various configurations of HES have been examined and found the optimal solution. The findings revealed that the power exchange with the grid could be minimized by the proposed HES (Wu et al. 2020).

A detailed literature survey reveals that, while integrating different types of renewable energy sources, it is essential to assess different facets of energy sources, such as technical, financial, and certain other external aspects, in order to obtain the optimum configuration of HES. In recent times, intelligent approaches have become more popular and are able to produce remarkable results. Most of the analysis related to grid-connected scenarios has been done using simulation tools like HOMER, etc. Comparatively, less research is available for grid-integrated HES using intelligent approaches. Further, biogas and biomass-based power generation have been rarely considered by researchers, which are important and potentially valuable resources, particularly in rural areas. Due to this circumstance, there is a research gap and a lack of specialized work in HES by selecting the optimal hybrid configuration depending on the renewable energy resources at a specific site by evaluating various economic and technical factors, etc. Hence, recognizing all these facts, the goal of this proposed work is to select the optimum configuration and sizing of the different components employed in the HES through different intelligent methodologies, viz., an improved HS named as IHS, a newly developed approach, and PSO, for the study area located in the northern region of India (Haryana).

2 Methodology

2.1 Site Selection

A group of four villages (Khanpur Kalan, Kakana, Kasanda, and Sargathal) situated in the district of Sonipat, Haryana state, has been considered in the present study. These villages are located at the latitude of 29.00 °N–29.15 °N and the longitude of 76.75 °E–77.01 °E (Anand et al. 2019a).

2.2 Assessment of Renewable Energy Resources at Selected Site

A comprehensive investigation was carried out to estimate the potential of renewable energy resources for the selected site. The collected data are shown in Table 1, which reveals that the study area has a huge potential for different renewable energy resources. These resources can be used to meet all of the energy needs of the rural people of that area. However, the annual average wind speed of 3 m/s available in the study area is not sufficient for power generation. Biomass has the maximum potential, followed by biogas and solar energy. Further, Khanpur Kalan village has the maximum potential for renewable energy resources among all villages in the study area. Therefore, this village has been chosen for the installation of a renewable energy-based power generation system.

2.3 Electrical Load Demand Assessment

To design a hybrid model for electrification of the considered site, the electrical load demand has been estimated by keeping in mind the living standards of the local people and the possible types of electrical appliances to be used by them. The average monthly temperature of the research area during the year lies from 4 to 46 °C. This variability in the study area's average temperature and climatic conditions influences the energy pattern used by different appliances. Therefore, for the present study, the whole year has been sub-divided into three seasons, such as the summer season (April–July), the moderate season (August–November) and the winter season (December–March). Further, the electrical load is characterized as municipal/governmental premises, commercial, residential, and agricultural loads. The residential load of 533 households in the study area includes loads like a fan, LED, TV, refrigerator, mobile charger, cooler, and water pump, etc., as shown in Table 2. The load demands of the school, health centre, veterinary hospital, and street lights are incorporated into the category of Municipal/Governmental load. Shops and water lift pumps are involved in commercial and agricultural loads, respectively.

The daily demand for energy for the research area during the summer season, moderate season, and winter season is computed as 2997.58 kWh/day, 2357.98 kWh/day, and 1286.149 kWh/day, respectively. The annual energy consumption for the chosen location is computed as 809,002.4 KWh/year.

Table 1 Assessment of potential of renewable energy resources at selected areas

Village	Available solar energy (kWh/m^2/day)	Available wind energy	Available biomass (crop residues)	Availability of biogas (cattle no.)
Khanpur Kalan	5.26	Average annual wind Speed = 3.27 m/s	1177.76 tonnes/year	Buffalo-3347 Cow-231 Sheep-123 Goat-17
Kasanda	5.24	–	550.61 tonnes/year	Buffalo- 797 Cow- 131 Sheep-0 Goat-15
Kakana	5.24	–	506.38 tonnes/year	Buffalo- 611 Cow- 51 Sheep-31 Goat-09
Sargathal	5.14	–	836.06 tonnes/year	Buffalo- 2062 Cow- 94 Sheep-32 Goat-11
Annual energy potential of the study area	1919.9 kWh/m^2/year for Khanpur Kalan	–	2,791,645.45 kWh/year	1,416,484.70 kWh/year

2.4 Objective Function with Design Constraints

The present research aims to minimize the NPC of the proposed system, described as:

Min. NPC

$$\mathrm{NPC} = \mathrm{NPC}_{\mathrm{PV}} + \mathrm{NPC}_{\mathrm{W}} + \mathrm{NPC}_{\mathrm{M}} + \mathrm{NPC}_{\mathrm{G}} + \mathrm{NPC}_{\mathrm{B}} + \mathrm{NPC}_{\mathrm{inv}} - C_{\mathrm{GS}} + C_{\mathrm{GP}} \tag{1}$$

where $\mathrm{NPC}_{\mathrm{PV}}$, $\mathrm{NPC}_{\mathrm{W}}$, $\mathrm{NPC}_{\mathrm{M}}$, $\mathrm{NPC}_{\mathrm{G}}$, $\mathrm{NPC}_{\mathrm{B},}$ and $\mathrm{NPC}_{\mathrm{inv}}$ represent the net present cost of the SPV system, wind energy system, biomass generator, biogas generator, battery, and inverter, respectively. C_{GS} defines the selling price of excess electricity to be sold to the utility grid, and C_{GP} represents the cost of deficient electricity to be purchased from the utility grid.

This NPC shall be minimized subjected to the various constraints on the system components as described in the subsequent sections.

2.4.1 Description of System Components

The size of the system components, i.e., the number of SPV panels (N_{PV}), number of batteries (N_{B}), power of biomass generators (P_{M}) and power of biogas generators (P_{G}), varies according to the load demand in the proposed system. The lower and upper limits of these components are, therefore, specified as:

$$N_{\mathrm{PV}} = \text{Integer}, N_{\mathrm{PV}}^{\mathrm{Mn}} \le N_{\mathrm{PV}} \le N_{\mathrm{PV}}^{\mathrm{Mx}}$$

$$N_{\mathrm{B}} = \text{Integer}, N_{\mathrm{B}}^{\mathrm{Mn}} \le N_{\mathrm{B}} \le N_{\mathrm{B}}^{\mathrm{Mx}}$$

$$P_{\mathrm{G}} = \text{Integer}, P_{\mathrm{G}}^{\mathrm{Mn}} \le P_{\mathrm{G}} \le P_{\mathrm{G}}^{\mathrm{Mx}}$$

$$P_{\mathrm{M}} = \text{Integer}, P_{\mathrm{M}}^{\mathrm{Mn}} \le P_{\mathrm{M}} \le P_{\mathrm{M}}^{\mathrm{Mx}}$$

2.4.2 Battery Storage Capacity Limits

For safe operation of the battery, the maximal (E_{Bmx}) and minimal (E_{Bmn}) energy storage capacity of the battery are considered and specified as:

$$E_{\mathrm{Bmn}} \le E_B(t) \le E_{\mathrm{Bmx}} \tag{2}$$

These battery storage capacity limiting values can be determined using the following Eqs. (3–4) (Anand et al. 2019a):

$$E_{\mathrm{Bmx}} = \frac{N_{\mathrm{B}} \times V_{\mathrm{B}} \times Q_{\mathrm{B}}}{1000} \times Q_{\mathrm{Bmx}} \tag{3}$$

$$E_{\mathrm{Bmn}} = \frac{N_{\mathrm{B}} \times V_{\mathrm{B}} \times Q_{\mathrm{B}}}{1000} \times Q_{\mathrm{Bmn}} \tag{4}$$

where the V_{B} indicates the nominal voltage of the battery (V), the Q_{B} denotes battery capacity (Ah), and the Q_{Bmn} and Q_{Bmx} indicate the minimum and maximum battery state of charge, respectively.

2.4.3 Constraint for Power Reliability Evaluation

In this study, loss of power supply probability (LPSP) is presumed as a power reliability constraint. If the electrical load demand surpasses the available generation, the user may not have electricity. LPSP is therefore calculated by (Chauhan and Saini 2016):

$$\mathrm{LPSP} = \frac{\text{Non served load at hour (t)}}{\text{Total load at hour (t)}} \tag{5}$$

The LPSP range is considered from 0 to 1. Also, the maximum and minimum limits for the LPSP are as follows:

$$0 \le \mathrm{LPSP} \le \mathrm{LPSP}^{\mathrm{mx}} \tag{6}$$

where $\mathrm{LPSP}^{\mathrm{mx}}$ is the LPSP's maximum limit. LPSP is assumed to be zero in the present work.

Table 2 Assessment of load demand for selected area

Load	Appliances	Rating (W)	Quantity/household	Operating hours			Summer season (kWh/day)	Moderate season (kWh/day)	Winter season (kWh/day)
				Summer season	Moderate season	Winter season			
Residential	LED light	12	3	04	04	04	0.144	0.144	0.144
	Fan	45	3	2@16 + 01@7	2@16 + 01@7	00	1.755	1.755	00
	TV	70	1	06	06	06	0.42	0.42	0.42
	Refreigerator	200	1	08	08	07	1.6	1.6	1.4
	Cooler	100	1	12	00	00	1.2	00	00
	Mobile charger	6	1	02	02	02	0.012	0.012	0.012
	Water pump	500	1	04	04	04	44.4	44.4	44.4
	Total daily energy consumption @ 533 households of the study area						2779.223	2139.623	1097.608
Municipal/governmental									
Health centre	LED light	12	2	12	12	12	0.288	0.288	0.288
	Fan	45	2	09	09	00	0.81	0.81	0
	Refrigerator	200	1	08	08	08	1.6	1.6	1.6
	Water heater	1000	1	03	03	03	3	3	3
	Total @ 4 villages						22.792	22.792	19.552
Veterinary hospital	LED light	12	2	12	12	12	0.288	0.288	0.288
	Fan	45	2	09	09	00	0.81	0.81	0
	Refrigerator	200	1	10	10	10	2	2	2
	Miscellaneous medical equipments	–	–	–	–	–	4.822	4.822	5.108
	Total @ 4 villages each of study area						31.68	31.68	32.584
School	LED light	12	10@each village	09	09	09	0.964	0.964	0.885
	Fan	45	10@ each village	09	09	00	0.405	0.405	0
	Total @ 4 villages	20.085	20.085	3.405					
Street lights	LED light	30	89@study area	12	12	12	32.04	32.04	32.04
	Daily energy consumption for Municipal/ Governmental load for the study area (kWh/day)						106.597	106.597	87.581
Agricultural	Water lifting pump	2500	10@ 4villages	4	4	4	100	100	100
	Total energy requirement per day @4villages each of study area						100	100	100
Commercial load (Shop)	LED	12	1@1shop	4	4	4	0.048	0.048	0.048
	Fan	45	1@1shop	12	12	00	0.54	0.54	00
	Total energy requirement per day @ 20 shops each of study area						11.76	11.76	0.96
Annual energy consumption of study area (kWh/year)							809,002.4		

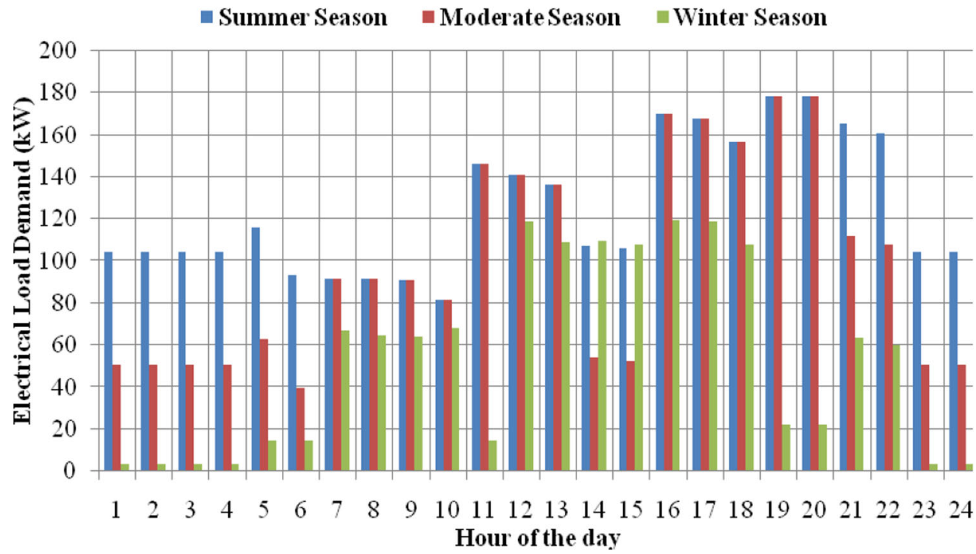

Fig. 1 Electrical load demand of the proposed location

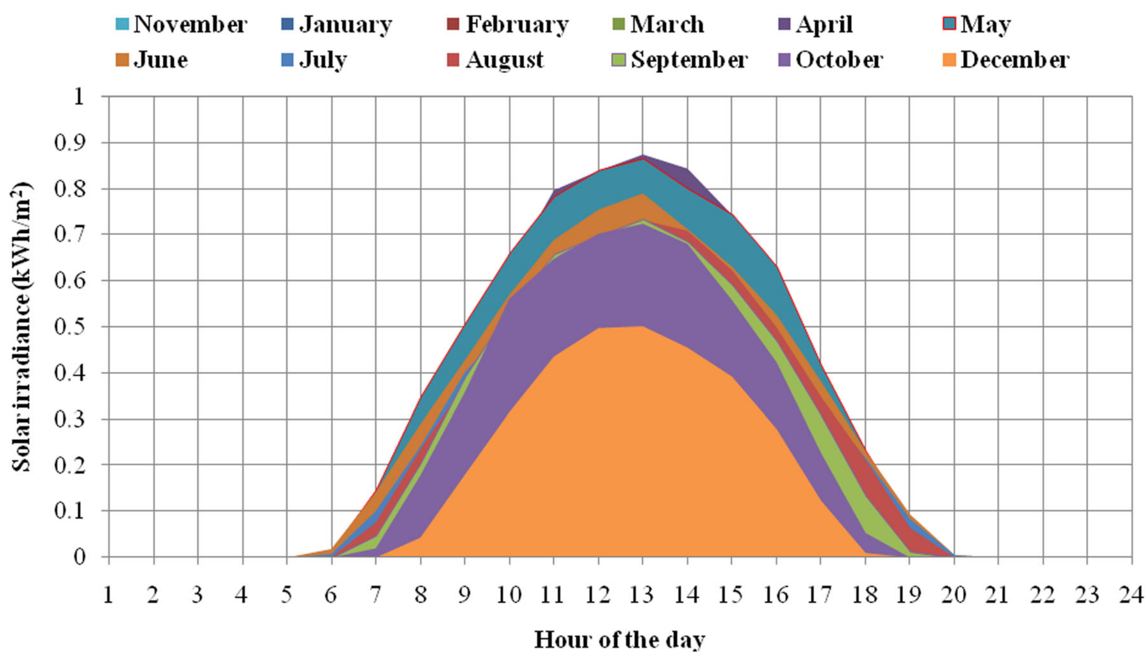

Fig. 2 Available monthly average solar energy for study area

2.5 IHS-based Intelligent Approach

HS has gained popularity in the past few decades as an efficient solution for solving difficult optimization issues. In the existing HS algorithm, the final position obtained from the harmony memory is utilized toward the location of the search space that is directed toward finding the optimal solution (Askarzadeh 2013b, a; Kamboj et al. 2016). This action may lead to a trap in the local optimum solution. Another offshoot is the reduction of the diversity of the population and HS to drop into the local optimum. To overcome these impediments, an improved harmony search (IHS) algorithm is proposed. The advancement includes a novel search strategy allied by selecting and amending steps, which consists of a dimension learning-based hunting (DLH) search strategy. In the IHS algorithm strategy, each individual harmony memory is well-read by its neighbors to be one more candidate for the latest position of $X_i(t)$. The steps below show how the standard HS and DLH search techniques produce two distinct candidates.

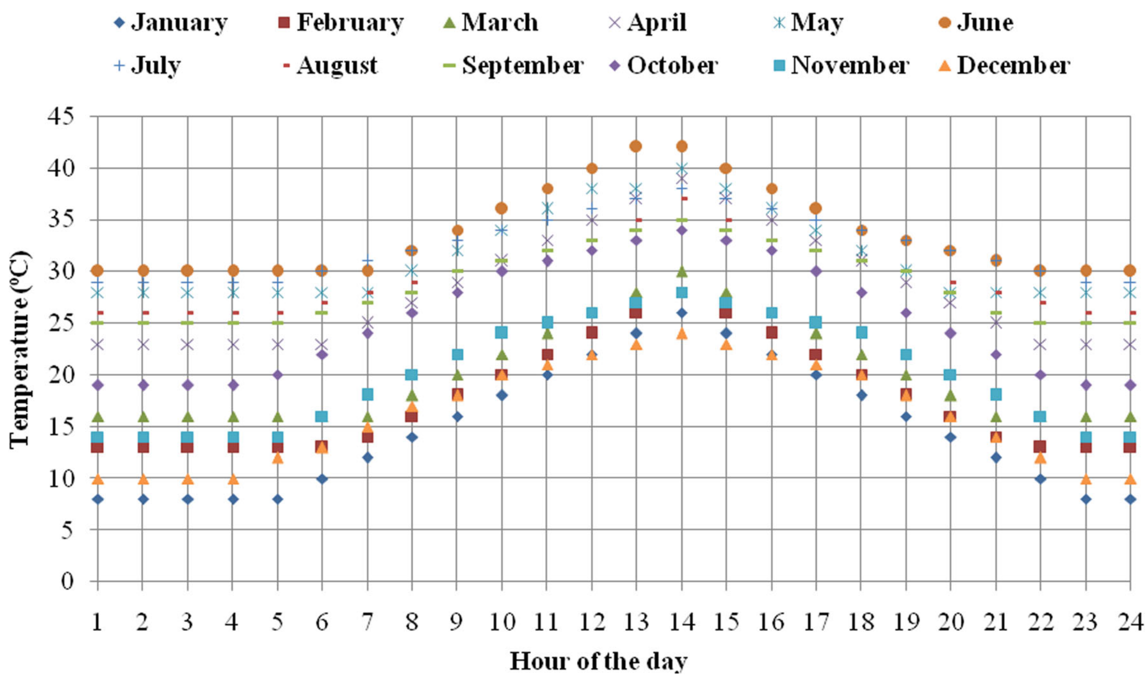

Fig. 3 Available mean air temperature for study area

Table 3 Scheduling of biogas and biomass generator for study area

Bio-generator	Summer season	Moderate season	Winter season
Biogas generator	01.00–05.00 am	01.00–05.00 am	17.00–19.00 pm
Biomass generator	18.00–24.00 pm	16.00–24.00 pm	20.00–22.00 pm

Table 4 Database of hybrid system (Anand et al. 2019b, 2020)

A system with the considered capacity	Capital cost ($)	O&M cost ($)	Salvage value ($)	Fuel cost
SPV system (235 W)	166.4	3.328	16.64	–
Biomass generator (1 kW)	895.2667	44.763	268.58	13$/tonne
Biogas generator (1 kW)	572	28.6	171.6	6.93 $/tonne

Table 5 Result of hybrid renewable energy system for off-grid scenario

Model	Algorithm	N_{PV} (nos.)	N_B (nos.)	P_{PV} (kW)	E_B (kWh)	P_M (kW)	P_G (kW)	NPC (10^5 $)	CoE ($/kWh)
M_{11}	IHS	975	227	229.13	544.8	166	-	7.17	0.105
	PSO	939	250	220.67	600	170	–	7.47	0.110
M_{12}	IHS	962	235	226.07	564	–	168	8.20	0.120
	PSO	912	268	214.32	643.2	–	173	8.64	0.127
M_{13}	IHS	804	356	188.94	854.4	179	216	11.95	0.175
	PSO	713	408	167.55	979.2	249	127	12.22	0.179

Table 6 Results of grid-connected model using IHS and PSO algorithms

Algorithm	N_{PV}	N_B	P_{PV} (kW)	P_M (kW)	P_G (kW)	E_B (kWh)	NPC ($10^5$$)	CoE ($/kWh)
IHS	963	23	226.31	41	98	55.2	6.00	0.081
PSO	858	34	201.63	87	5	81.6	6.12	0.088

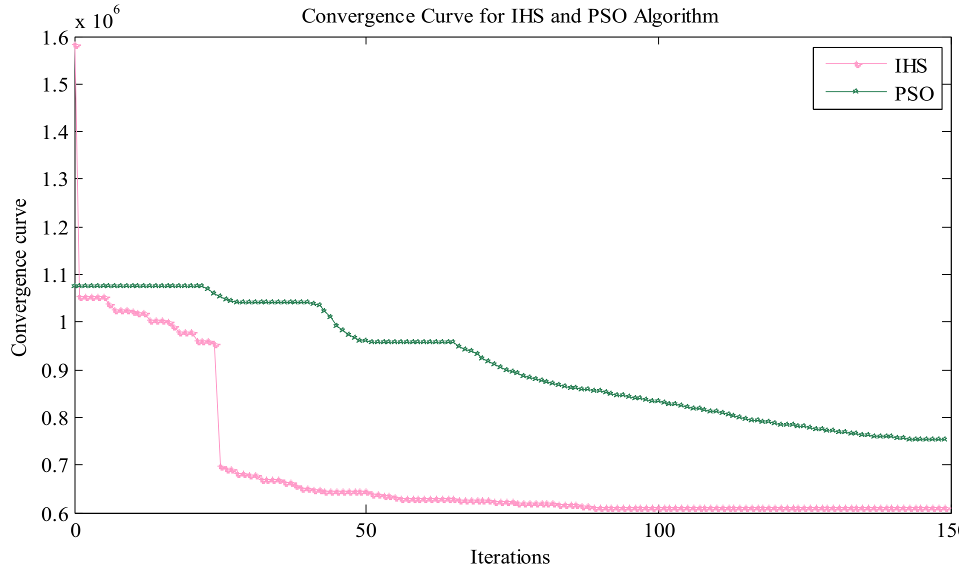

Fig. 4 Convergence curve of IHS and PSO algorithm for best model

DLH Search Strategy In the original HS, for each harmony memory, the latest position is produced from the given population. As a result of this, HS has a sluggish convergence rate, the population loses diversity too soon, and chimps get stuck in the local optima. To address these flaws, the suggested DLH search technique considers an individual local position that is learnt from its neighbors. Each dimension of the new location of harmony memory $X_i(t)$ is computed by Eq. (7a) in the DLH search strategy, in which this particular harmony memory is learnt by its various neighbors and a randomly picked population. Then, as well,$r_i(t)$, another candidate for the latest position of harmony memory $X_i(t)$ named $X_{I-\mathrm{DLH}}(t+1)$, is generated by the DLH search strategy. To achieve this, initially, a radius $r_i(t)$ is calculated by the Euclidean distance between the present positions of $X_i(t)$ and position $X_{\mathrm{IHS}}(t+1)$ by the Eq. (7b).

$$X_{i-\mathrm{DLH},d}(t+1) = X_{i,d}(t) + \mathrm{rand} \times \left(X_{n,d}(t) - X_{r,d}(t)\right) \tag{7a}$$

$$r_i(t) = \|X_i(t) - X_{\mathrm{IHS}}(t+1)\| \tag{7b}$$

Then, the neighbors of $X_i(t)$ represented by $\mathrm{N_i(t)}$ are constructed by Eq. (7c) with respect to $r_i(t)$, where D_i is the Euclidean distance between $X_i(t)$ and $X_j(t)$.

$$N_i(t) = \left\{X_j(t)\, D_i\left(X_i(t), X_j(t)\right) \le r_i(t), X_j(t) \in \mathrm{Pop}\right\} \tag{7c}$$

Once the neighborhood of $\mathrm{X_i(t)}$ is constructed, multi-neighborhood learning is performed by Eq. (7a), where the dth dimension of $X_{I-\mathrm{DLH},d}(t+1)$ is determined by using the dth dimension of a random neighbor $X_{n,d}(t)$ selected from $N_i(t)$, and a random harmony $X_{r,d}(t)$ from the population (Pop).

Attacking Phase In this phase, first the superior candidate is elected by comparing the fitness values of two candidates $X_{IHS}(t+1)$ and $X_{I-DLH}(t+1)$ by the Eq. (7a).

Then, in order to update the latest position of $\mathrm{X_i(t + 1)}$, if the fitness value of the selected candidates is less than $\mathrm{X_i(t)}$, $\mathrm{X_i(t)}$ is updated by the elected candidate. Otherwise, $\mathrm{X_i(t)}$ remains unchanged in the population.

$$X_i(t+1) = \begin{cases} X_{\mathrm{IHS}}(t+1)\,; & if\, f\,(X_{\mathrm{IHS}}) < f(X_{I-\mathrm{DLH}}(t+1) \\ X_{I-\mathrm{DLH}}(t+1); & \text{otherwise} \end{cases} \tag{7d}$$

Finally, after repeating this method for all individuals, the iteration counter is incremented by one, and the search can be repeated until the predetermined number of iterations is reached.

The step-wise method of implementing the IHS algorithm for optimization is discussed below.

2.5.1 Problem Formulation

The problem of optimization concerning an objective function f(X) can be expressed as:

Min. f(X) subject to

$$x_i^{\mathrm{mn}} \le x_i \le x_i^{\mathrm{mx}} (i = 1, 2, 3, 4, \ldots, n)$$

where X = [× 1, × 2, × 3,…xn]$^{\mathrm{T}}$ denotes a set of decision variables and n denotes the number of decision variables or problem dimensions.

Furthermore, various steps are summarized for implementing the IHS code as:

Table 7 Test result of UM benchmark functions using IHS algorithm for 10, 30, 50, and 100 dimensions

Function no	Parameters	Objective fitness function (10 dimensions)	Objective fitness function (30 dimensions)	Objective fitness function (50 dimensions)	Objective fitness function (100 dimensions)
F1	Index	1	14	27	20
	Mean	1.46E-190	6.02E-31	0.0006159	0.0237249
	SD	0	3.30E-30	0.0016309	0.0080498
	Best	0	1.61E-160	1.41E-63	0.0090996
	Worst	4.37E-189	1.81E-29	0.0076871	0.0397484
	Median	0	3.02E-79	2.97E-22	0.0245168
F2	Index	1	1	27	30
	Mean	0	0	1.73E-178	2.89E-65
	SD	0	0	0	1.58E-64
	Best	0	0	1.47E-257	2.55E-119
	Worst	0	0	5.17E-177	8.66E-64
	Median	0	0	1.16E-227	3.37E-90
F3	Index	1	5	2	21
	Mean	0	0.0062922	0.0737742	0.7291939
	SD	0	0.0117352	0.0414089	0.4417872
	Best	0	4.09E-119	0.0023466	0.3250389
	Worst	0	0.0520213	0.1748615	2.3129826
	Median	0	5.31E-22	0.0686605	0.5454504
F4	Index	2	15	12	19
	Mean	2.74E-54	0.0256386	0.0489318	0.0885322
	SD	1.50E-53	0.0202212	0.0143959	0.0092894
	Best	0	2.89E-49	4.13E-06	0.0685978
	Worst	8.22E-53	0.0486136	0.0696788	0.113581
	Median	0	0.0394833	0.050245	0.0876076
F5	Index	29	13	4	21
	Mean	6.5581064	28.457134	48.732954	98.867182
	SD	0.3960093	0.2924578	0.1834307	0.1165037
	Best	5.8098523	27.656336	48.39324	98.528255
	Worst	7.4484759	28.90474	48.939714	98.984317
	Median	6.5147293	28.471396	48.771238	98.921066
F6	Index	27	26	1	22
	Mean	0.0275005	3.1746032	7.1810491	18.312907
	SD	0.0133937	0.2849396	0.3985647	0.5881708
	Best	0.0114381	2.5403941	6.4545206	16.694277
	Worst	0.0679568	3.7000377	7.8438373	19.282699
	Median	0.0265952	3.2477819	7.2347066	18.455543
F7	Index	5	11	7	3
	Mean	6.09E-05	6.37E-05	6.22E-05	4.26E-05
	SD	6.83E-05	8.20E-05	7.37E-05	4.35E-05
	Best	1.95E-06	2.22E-06	8.83E-07	1.73E-06
	Worst	0.0002827	0.0004361	0.0003747	0.0001775
	Median	3.58E-05	5.27E-05	4.31E-05	2.23E-05

Table 8 Quartile result for UM function using IHS algorithm (10, 30, 50, 100 dimensions)

Dimension	Function no	No. of trials	Minimum value	Maximum value	Mean value	Median	First quartile (25th percentile)	Second quartile (50th percentile)	Third quartile (75th percentile)	Semi interquartile deviation	Number of outliers	SD
10 Dimensions	F1	30	0	4.3648E-189	1.4549E-190	0		0	4.3648E-189		0	0
	F2	30	0	0	0	0		0			0	0
	F3	30	0	0	0	0		0			0	0
	F4	30	0	8.22215E-53	2.74072E-54	0		0	1.1925E-269		0	1.50115E-53
	F5	30	5.809852328	7.448475875	6.558106427	6.514729312	6.288813448	6.514729312	6.793622776	0.252404664	0	0.396009329
	F6	30	0.011438088	0.067956753	0.027500504	0.026595237	0.018135659	0.026595237	0.029940686	0.005902514	3	0.013393713
	F7	30	1.94646E-06	0.000282693	6.08616E-05	3.58428E-05	1.29907E-05	3.58428E-05	8.72366E-05	3.71229E-05	2	6.83318E-05
30 Dimensions	F1	30	1.6105E-160	1.80523E-29	6.01744E-31	3.02488E-79	1.5311E-104	3.02488E-79	6.6906E-62	3.3453E-62	7	3.29589E-30
	F2	30	0	0	0	0		0			0	0
	F3	30	4.0886E-119	0.052021312	0.006292177	5.30962E-22	4.78228E-78	5.30962E-22	0.010746351	0.005373176	1	0.011735228
	F4	30	2.89447E-49	0.048613587	0.025638632	0.039483265	2.07579E-10	0.039483265	0.042362411	0.021181205	0	0.020221207
	F5	30	27.65633646	28.90474044	28.4571341	28.47139603	28.31293653	28.47139603	28.68209977	0.184581621	0	0.292457848
	F6	30	2.540394098	3.700037676	3.174603238	3.247781907	2.943327666	3.247781907	3.397659975	0.227166155	0	0.28493956
	F7	30	2.21967E-06	0.000436051	6.37432E-05	5.2654E-05	1.75343E-05	5.2654E-05	7.76907E-05	3.00782E-05	1	8.19746E-05
50 Dimensions	F1	30	1.41E-63	0.007687	0.000616	2.97E-22	2.4E-33	2.97E-22	1.61E-13	8.06E-14	7	0.001631
	F2	30	1.5E-257	5.2E-177	1.7E-178	1.2E-227	8.9E-248	1.2E-227	1.4E-214	7.2E-215	7	0
	F3	30	0.002347	0.174862	0.073774	0.068661	0.042973	0.068661	0.104216	0.030621	0	0.041409
	F4	30	4.13E-06	0.069679	0.048932	0.050245	0.045284	0.050245	0.05869	0.006703	1	0.014396
	F5	30	48.39324	48.93971	48.73295	48.77124	48.57573	48.77124	48.90579	0.165032	0	0.183431
	F6	30	6.454521	7.843837	7.181049	7.234707	6.916985	7.234707	7.492536	0.287775	0	0.398565
	F7	30	8.83E-07	0.000375	6.22E-05	4.31E-05	2.03E-05	4.31E-05	7.78E-05	2.87E-05	2	7.37E-05
100 Dimensions	F1	30	0.0091	0.039748	0.023725	0.024517	0.017495	0.024517	0.028955	0.00573	0	0.00805
	F2	30	2.6E-119	8.66E-64	2.89E-65	3.37E-90	4.24E-98	3.37E-90	1.33E-82	6.64E-83	7	1.58E-64
	F3	30	0.325039	2.312983	0.729194	0.54545	0.423132	0.54545	0.999589	0.288228	1	0.441787
	F4	30	0.068598	0.113581	0.088532	0.087608	0.082573	0.087608	0.094731	0.006079	0	0.009289
	F5	30	98.52826	98.98432	98.86718	98.92107	98.82575	98.92107	98.93731	0.055777	0	0.116504
	F6	30	16.69428	19.2827	18.31291	18.45554	18.08796	18.45554	18.67388	0.292962	0	0.588171
	F7	30	1.73E-06	0.000177	4.26E-05	2.23E-05	1.12E-05	2.23E-05	8.17E-05	3.53E-05	0	4.35E-05

Table 9 Test result of UM benchmark functions using IHS algorithm for 10, 30, 50 and 100 dimensions

Function no	Parameters		Objective fitness function (10 dimensions)	Objective fitness function (30 dimensions)	Objective fitness function (50 dimensions)	Objective fitness function (100 dimensions)
F1	Wilcoxon rank sum test	*p*-rank	0.3337107	0.06786886	0.0678689	0.63087629
		h-rank	0	0	0	0
	T-Test	*p*-test	1	0	0	0
		t-test	0	0.32557885	0.2303897	0.81708626
F2	Wilcoxon rank sum test	*p*-rank		–	0.8418015	0.78445977
		h-rank	0	0	0	0
	T-Test	*p*-test	–	–	0	0
		t-test	–	–	0.325582	0.32556084
F3	Wilcoxon rank sum test	*p*-rank	0.3337107	0.6843226	0.9823071	0.37107703
		h-rank	0	0	0	0
	T-Test	*p*-test	1	0	0	0
		t-test	0	0.4847723	0.2455422	0.15629828
F4	Wilcoxon rank sum test	*p*-rank	0.4320441	0.3790363	0.807275	0.14127751
		h-rank	0	0	0	0
	T-Test	*p*-test	0	0	0	0
		t-test	0.325582	0.5461467	0.5340496	0.07345329
F5	Wilcoxon rank sum test	*p*-rank	0.3870998	0.6204037	0.3041768	0.85338174
		h-rank	0	0	0	0
	T-Test	*p*-test	0	0	0	0
		t-test	0.4133304	0.6706703	0.4845669	0.58682251
F6	Wilcoxon rank sum test	*p*-rank	0.0270863	0.4464194	0.5996895	0.30417682
		h-rank	1	0	0	0
	T-Test	*p*-test	1	0	0	0
		t-test	0.0197353	0.5211085	0.4738117	0.54989648
F7	Wilcoxon rank sum test	*p*-rank	0.5996895	0.935192	0.040595	0.00058737
		h-rank	0	0	1	1
	T-Test	*p*-test	0	0	0	1
		t-test	0.7710415	0.7596276	0.1515444	0.00143501

2.5.2 IHS Parameter Initialization

Adjustable IHS parameters, which include Harmony Memory Size (HMS), Pitch Rate (PR), Harmony Memory Consideration Rate (HMR), and Generation Bandwidth (BW), are also initialized.

The initialization of elements of the harmony memory matrix is done by using the following equation.

$$X_{ij} = X_{\mathrm{i}}^{\mathrm{mn}} + \mathrm{rand}\ (X_i^{\mathrm{mx}} - X_i^{\mathrm{mn}}) \tag{8a}$$

where j = 1,2,3, 4…n; i = 1,2,3,4……HMS. where X_i^{mx} and $\mathrm{X}_{\mathrm{i}}^{\mathrm{mn}}$ denote upper and lower bounds on ith decision variable; rand denotes random values distributed in the 0–1 range. Mathematically, the harmony memory (HM) matrix is represented as:

$$\mathrm{HM} = \begin{bmatrix} x_{11} & x_{12} & x_{13} & \ldots\ldots\ldots x_{1n} \\ x_{21} & x_{22} & x_{23} & \ldots\ldots\ldots x_{2n} \\ x_{31} & x_{32} & x_{33} & \ldots\ldots\ldots x_{3n} \\ . & & & \\ . & & & \\ x_{\mathrm{HMS1}} & x_{\mathrm{HMS2}} & x_{\mathrm{HMS3}} & \ldots\ldots\ldots x_{\mathrm{HMS}n} \end{bmatrix}_{\mathrm{HMS}\times n} \tag{8b}$$

2.5.3 Development of New Harmony

A new harmony vector is developed based on experience and is referred to as improvisation or adjustment of harmony. To generate new harmony, i.e., *X*nw = [xnw, 1, xnw, 2, xnw, 3,…xnw, n], the following stages are carried out for all decision variables:

Table 10 Simulation time of UM benchmark functions using IHS algorithm for 10, 30, 50 and 100 dimensions

Function no	Parameters	Objective fitness function (10 dimensions)	Objective fitness function (30 dimensions)	Objective fitness function (50 dimensions)	Objective fitness function (100 dimensions)
F1	Best time (Sec)	0.03125	0.046875	0.078125	0.140625
	Average time (Sec.)	0.078125	0.1020833	0.1416667	0.2223958
	Worst time (Sec)	0.25	0.328125	0.421875	0.90625
F2	Best time (Sec)	0.03125	0.0625	0.078125	0.140625
	Average time (Sec.)	0.0776042	0.1041667	0.125	0.2015625
	Worst time (Sec)	0.34375	0.3125	0.375	0.5625
F3	Best time (Sec)	0.0625	0.171875	0.28125	0.59375
	Average time (Sec.)	0.0942708	0.1973958	0.3276042	0.65625
	Worst time (Sec)	0.171875	0.234375	0.859375	0.875
F4	Best time (Sec)	0.03125	0.0625	0.078125	0.140625
	Average time (Sec.)	0.0651042	0.0895833	0.1125	0.1572917
	Worst time (Sec)	0.140625	0.1875	0.1875	0.203125
F5	Best time (Sec)	0.046875	0.0625	0.09375	0.140625
	Average time (Sec.)	0.08125	0.0807292	0.1145833	0.1723958
	Worst time (Sec)	0.140625	0.109375	0.15625	0.359375
F6	Best time (Sec)	0.03125	0.0625	0.078125	0.125
	Average time (Sec.)	0.0619792	0.071875	0.0994792	0.1614583
	Worst time (Sec)	0.09375	0.109375	0.171875	0.265625
F7	Best time (Sec)	0.0625	0.109375	0.171875	0.328125
	Average time (Sec.)	0.0848958	0.1296875	0.2088542	0.3432292
	Worst time (Sec)	0.125	0.171875	0.3125	0.375

Stage (i): A new random number (RN) is generated in the range of 0–1.

If RN > HMR, then the decision variable X_{ij}^{nw} is generated by using the following equation.

$$X_{ij}^{\mathrm{nw}} = X_j^{\mathrm{mn}} + \mathrm{rand}\ (X_j^{\mathrm{mx}} - X_j^{\mathrm{mn}}) \tag{9}$$

where j = 1,2,3, 4…….n; i = 1,2,3,4……HMS.

If, on the contrary, $\mathrm{RN} \le \mathrm{HMR}$, then one of the decision variables stored in the current HM is chosen at random using the following equation:

$$X_{ij}^{\mathrm{nw}} = X_{ij} \tag{10}$$

where i = 1,2,3,4……HMS; j = 1,2,3,4…….n;

Stage (ii): HS considers a pitch adjustment mechanism through which the new harmony can move to a neighboring value in respect of the possible range. To execute a pitch adjustment mechanism, a uniformly distributed random number (rand) is generated between 0 and 1 after stage (i). If $\mathrm{rand} \le \mathrm{PR}$, the new harmony will move to a neighboring value using the following equation.

$$X_{ij}^{\mathrm{nw}} = X_{ij}^{\mathrm{nw}} + B_{\mathrm{W}} \times (\mathrm{rand}{-}0.5) \times (X_j^{\mathrm{mn}} {-} X_j^{\mathrm{mx}}) \tag{11}$$

where B_{W} denotes bandwidth;

Further, the iteration-wise value of variables PR and $\mathrm{B_W}$ is calculated as follows (Anand et al. 2020):

$$\mathrm{PR(itr)} = \mathrm{PR_{mn}} + \frac{(\mathrm{PR_{mx}} - \mathrm{PR_{mn}})}{\mathrm{itr_{mx}}} \times (\mathrm{itr}) \tag{12}$$

$$B_{\mathrm{W}}(\mathrm{itr}) = B_{\mathrm{Wmx}} \exp\ (\mathrm{a.itr})$$

$$a = \frac{\mathrm{Ln}\left(\frac{B_{\mathrm{wmn}}}{B_{\mathrm{wmx}}}\right)}{\mathrm{itr_{mx}}} \tag{13}$$

where PR (itr) represents an iteration wise pitch adjustment rate; itr denotes an iteration index; $\mathrm{PR_{mx}}$ and $\mathrm{PR_{mn}}$ denote the maximum and minimum value of the adjustment rate of the pitch. B_{Wmx} and B_{Wmn} denote maximum and minimum bandwidth values.

Stage (iii): The population obtained from Eq. (11) is further updated using a DLH-based search strategy.

2.5.4 Updation

If the newly created harmony vector $\left(X_{ij}^{\mathrm{nw}}\right)$ delivers better results as compared to the worst $\left(X_{ij}^{\mathrm{wst}}\right)$ harmony in HM, the new harmony vector is taken into account in the HM

Table 11 Test result of MM benchmark functions using IHS algorithm for 10, 30, 50 and 100 dimensions

Function no	Parameters	Objective fitness function (10 dimensions)	Objective fitness function (30 dimensions)	Objective fitness function (50 dimensions)
F8	Index	23	8	19
	Mean	− 2850.43	− 5121.3336	− 6972.8981
	SD	257.17714	443.84981	432.78124
	Best	− 3367.3551	− 6437.3229	− 7778.3714
	Worst	− 2372.6406	− 4317.8725	− 5883.5459
	Median	− 2859.3609	− 5090.4497	− 7012.4868
F9	Index	1	1	1
	Mean	0	0	0
	SD	0	0	0
	Best	0	0	0
	Worst	0	0	0
	Median	0	0	0
F10	Index	1	1	1
	Mean	8.88E-16	8.88E-16	8.88E-16
	Std	0	0	0
	Best	8.88E-16	8.88E-16	8.88E-16
	Worst	8.88E-16	8.88E-16	8.88E-16
	Median	8.88E-16	8.88E-16	8.88E-16
F11	Index	1	22	3
	Mean	3.71E-12	0.1893664	1.287844
	SD	2.03E-11	0.1376684	0.6147181
	Best	0	0.0179498	0.4657037
	Worst	1.11E-10	0.4722641	3.4812008
	Median	0	0.1714668	1.0759526
F12	Index	1	25	8
	Mean	0.0276916	0.5100072	0.7308314
	SD	0.0069211	0.0432966	0.0271067
	Best	0.0161779	0.4211718	0.6672053
	Worst	0.0443696	0.5921292	0.7781942
	Median	0.0279344	0.5134917	0.7370376
F13	Index	14	18	16
	Mean	0.8602966	2.8308818	4.8618731
	SD	0.1285511	0.0915252	0.1038929
	Best	0.5495171	2.5571825	4.6639295
	Worst	0.9956581	2.9969841	5.0109654
	Median	0.8844531	2.8306134	4.8740007

instead of the existing worst harmony and it is mathematically represented as:

$$X_{ij}^{\mathrm{wst}} = \left\{ \begin{array}{ll} X_{ij}^{\mathrm{new}}; & f\left(X_{ij}^{\mathrm{new}}\right) < f\left(X_{ij}^{\mathrm{wst}}\right) \\ X_{ij}^{\mathrm{wst}}; & \text{Otherwise} \end{array} \right\} \tag{14}$$

Based on the obtained solution, the best value of the objective function is calculated as:

$$f^{\mathrm{bst}} = \min\left(f_i\right);\ i \in 1, 2, 3, 4\ldots\ldots\mathrm{HMS} \tag{15}$$

2.5.5 Check Stopping Criteria

If no. of iterations exceeds, then the algorithm will cease to work, else step 2.5.3 and step 2.5.4 are repeated.

2.6 PSO-based Intelligent Approach

PSO is a stochastic-based optimization approach that has been propelled by the communal performance of bird congregating, which initializes with inhabitants of random

Table 12 Quartile result for MM test function using IHS (10, 30, 50, 100 dimensions)

Dimension	Function no	No. of trials	Minimum value	Maximum value	Mean value	Median	First quartile (25th percentile)	Second quartile (50th percentile)	Third quartile (75th percentile)	Semi interquartile deviation	Number of outliers	SD
10 Dimensions	F8	30	− 3367.355	− 2372.641	− 2850.43	− 2859.361	− 3031.732	− 2859.361	− 2727.692	152.01969	0	257.17713
	F9	30	0	0	0	0	–	0	–	–	0	0
	F10	30	8.882E-16	8.882E-16	8.882E-16	8.882E-16	–	8.882E-16	–	–	0	0
	F11	30	0	1.114E-10	3.714E-12	0	–	0	5.571E-11	–	0	2.034E-11
	F12	30	0.0161779	0.0443696	0.0276916	0.0279343	0.0212042	0.0279343	0.0320797	0.0054377	0	0.0069211
	F13	30	0.5495171	0.9956581	0.8602966	0.8844531	0.844347	0.8844531	0.939061	0.047357	1	0.1285511
30 Dimensions	F8	30	− 6437.32	− 4317.87	− 5121.33	− 5090.45	− 5346.52	− 5090.45	− 4827.89	259.312	0	443.8498
	F9	30	0	0	0	0		0			0	0
	F10	30	8.88E-16	8.88E-16	8.88E-16	8.88E-16		8.88E-16			0	0
	F11	30	0.01795	0.472264	0.189366	0.171467	0.066652	0.171467	0.256276	0.094812	0	0.137668
	F12	30	0.421172	0.592129	0.510007	0.513492	0.47345	0.513492	0.538682	0.032616	0	0.043297
	F13	30	2.557182	2.996984	2.830882	2.830613	2.782429	2.830613	2.886724	0.052147	0	0.091525
50 Dimensions	F8	30	− 7778.37	− 5883.55	− 6972.9	− 7012.49	− 7218.73	− 7012.49	− 6689.36	264.6839	0	432.7812
	F9	30	0	0	0	0	–	0	–	–	0	0
	F10	30	8.88E-16	8.88E-16	8.88E-16	8.88E-16	–	8.88E-16	–	–	0	0
	F11	30	0.465704	3.481201	1.287844	1.075953	0.924716	1.075953	1.467026	0.271155	2	0.614718
	F12	30	0.667205	0.778194	0.730831	0.737038	0.714607	0.737038	0.747946	0.01667	0	0.027107
	F13	30	4.66393	5.010965	4.861873	4.874001	4.76689	4.874001	4.941805	0.087457	0	0.103893
100 Dimensions	F8	30	− 11,259.6	− 8075.02	− 9946.69	− 9959.65	− 10,554.4	− 9959.65	− 9626.94	463.7405	0	767.3219
	F9	30	0	0	0	0	–	0	–	–	0	0
	F10	30	8.88E-16	0.003568	0.000672	8.88E-16	0	8.88E-16	0.002077		0	0.001103
	F11	30	232.8222	927.7727	596.3999	589.2233	500.0965	589.2233	744.2696	122.0865	0	181.4274
	F12	30	0.857602	0.94594	0.903276	0.904086	0.887647	0.904086	0.917979	0.015166	0	0.021584
	F13	30	9.698846	10.02458	9.956183	9.968506	9.927189	9.968506	10.00467	0.038743	0	0.067823

Table 13 Test result of MM benchmark functions using IHS algorithm for 10, 30, 50 and 100 dimensions

Function no	Parameters		Objective fitness function (10 dimensions)	Objective fitness function (30 dimensions)	Objective fitness function (50 dimensions)	Objective fitness function (100 dimensions)
F8	Wilcoxon rank sum test	*p*-rank	0.9705161	0.0138316	0.6414235	0.2707053
		h-rank	0	1	0	0
	T-Test	*p*-test	0	1	0	0
		t-test	0.9132262	0.0199548	0.9380641	0.1097652
F9	Wilcoxon rank sum test	*p*-rank	–	–	–	–
		h-rank	0	0	0	0
	T-Test	*p*-test	–	–	–	–
		t-test	–	–	–	–
F10	Wilcoxon rank sum test	*p*-rank	–	–	–	0.6665651
		h-rank	0	0	0	0
	T-Test	*p*-test	–	–	–	0
		t-test		–	–	0.4702274
F11	Wilcoxon rank sum test	*p*-rank	0.9863612	0.5297825	0.7393988	0.8766349
		h-rank	0	0	0	0
	T-Test	*p*-test	0	0	0	0
		t-test	0.4305782	0.6253625	0.5604393	0.7591375
F12	Wilcoxon rank sum test	*p*-rank	0.6627348	0.7618283	0.077272	0.371077
		h-rank	0	0	0	0
	T-Test	*p*-test	0	0	0	0
		t-test	0.6191869	0.7865857	0.2418907	0.4122382
F13	Wilcoxon rank sum test	*p*-rank	0.395267	0.0451462	0.9823071	0.4289634
		h-rank	0	1	0	0
	T-Test	*p*-test	0	0	0	0
		t-test	0.6061278	0.0845897	0.8402802	0.7232989

solutions known as particles and sees the optimal solution by updating generation.

In PSO, the particle is represented by a vector having m decision variables. Initially, m particles are arbitrarily initialized in the search space. Each particle is trying to get a better position than the present one. The memory information comprises the best experience expressed by the group (G_{best}) and the best experience gained by the particle (P_{best}). The updating expression at each iteration (i) is given by the equation as (Anand et al. 2019a; Askarzadeh and Leandro 2015; Mahesh and Sandhu 2019):

$$V_j(i+1) = w \times V_j(i) + C_1 \times r_1\left(P_{\text{best}j}(i) - x_j(i)\right) + C_2 \times r_2\left(G_{\text{best}j}(i) - x_j(i)\right) \quad (16)$$

$$x_j(i+1) = V_j(i+1) + x_j(i) \quad (17)$$

where i = 1,2,3,.......i_{max}; j = 1,2,3,4......S_P. where V_j denotes the velocity of jth particle; x_j represents the position of jth particle; S_P denotes the size of particles; C_1 and C_2 are the learning coefficients; $r1$ and $r2$ represent random numbers lying in the range of 0 to 1; i_{max} is the maximum number of iterations.

Further, w known as inertia weight factor is used to provide a balance among the local and global search. A larger value of w results in a global search, whereas a small value leads to a local search. Generally, the value of w is varied by using the following equation.

$$w(i) = w_{mx} - \frac{w_{mx} - w_{mn}}{i_{max}} \times i \quad (18)$$

where w_{mn} and w_{mx} are the initial and final values of inertia weight.

Further, the following steps for implementing the PSO algorithm are described as:

2.6.1 Initialization of the Problem with PSO Parameters

The first step is to formulate the problem (objective function along with constraints). Besides, the adjustable PSO parameters are also defined.

Table 14 Simulation time of MM benchmark functions using IHS algorithm for 10, 30, 50 and 100 dimensions

Function no	Parameters	Objective fitness function (10 dimensions)	Objective fitness function (30 dimensions)	Objective fitness function (50 dimensions)	Objective fitness function (100 dimensions)
F8	Best time (Sec)	0.03125	0.078125	0.109375	0.171875
	Average time (Sec.)	0.0744792	0.0875	0.1338542	0.2067708
	Worst time (Sec)	0.15625	0.125	0.171875	0.3125
F9	Best time (Sec)	0.03125	0.0625	0.09375	0.140625
	Average time (Sec.)	0.0614583	0.0729167	0.1229167	0.1651042
	Worst time (Sec)	0.109375	0.125	0.1875	0.28125
F10	Best time (Sec)	0.046875	0.0625	0.09375	0.140625
	Average time (Sec.)	0.0640625	0.075	0.1177083	0.1682292
	Worst time (Sec)	0.09375	0.109375	0.203125	0.265625
F11	Best time (Sec)	0.046875	0.078125	0.109375	0.1875
	Average time (Sec.)	0.078125	0.0890625	0.1364583	0.2171875
	Worst time (Sec)	0.125	0.125	0.21875	0.28125
F12	Best time (Sec)	0.140625	0.234375	0.328125	0.59375
	Average time (Sec.)	0.1671875	0.265625	0.3651042	0.6244792
	Worst time (Sec)	0.25	0.3125	0.40625	0.640625
F13	Best time (Sec)	0.140625	0.234375	0.328125	0.578125
	Average time (Sec.)	0.1598958	0.2473958	0.36875	0.6005208
	Worst time (Sec)	0.1875	0.28125	0.421875	0.640625

2.6.2 Initialization of Particles

In the second step, m particles have been initialized in the search space with randomly generated decision vectors. The initialization of each particle is done using the following equation.

$$x(0) = x_{\mathrm{mn},j} + \mathrm{rand}\left(x_{\mathrm{mx},j} - x_{\mathrm{mn},j}\right) \tag{19}$$

where x_{mx} and x_{mn} denote the initial and final value of x for all particles.

2.6.3 Fitness Function Evaluation

Based on the value of decision variables associated with each particle, the value of the objective function is determined.

2.6.4 Updation

P_{best} is calculated for each particle and G_{best} is selected among the population based on the best particle. Further, each particle is allowed to move to the next new position. More specifically, the velocity of each particle and its

Table 15 Test result of FD benchmark functions using IHS algorithm for 10, 30, 50 and 100 dimensions

Function no	Parameters	Objective fitness function (10 dimensions)	Objective fitness function (30 dimensions)	Objective fitness function (50 dimensions)	Objective fitness function (100 dimensions)
F14	Index	20	30	17	27
	Mean	8.9586192	9.2958827	9.5502341	10.444576
	SD	4.6885511	3.708035	3.8707949	4.0003265
	Best	0.9980038	1.9920309	0.9980038	0.9980038
	Worst	12.670506	12.670506	12.670506	12.670506
	Median	11.7187	10.763181	10.763181	12.670506
F15	Index	26	29	8	–
	Mean	0.0160376	0.0169005	0.0181053	–
	SD	0.030964	0.0327302	0.0315364	–
	Best	0.0003475	0.0003475	0.000353	–
	Worst	0.1207472	0.1162259	0.1089183	–
	Median	0.0019117	0.0010714	0.0043061	–
F16	Index	28	30	6	–
	Mean	− 1.0316283	− 1.0316283	− 1.0316283	–
	SD	1.34E-07	1.15E-07	1.75E-07	–
	Best	− 1.0316285	− 1.0316284	− 1.0316284	–
	Worst	− 1.031628	− 1.031628	− 1.0316275	–
	Median	− 1.0316283	− 1.0316283	− 1.0316283	–
F17	Index	14	16	30	27
	Mean	0.4123419	0.4097653	0.4130562	0.4127692
	SD	0.0098248	0.010759	0.0138232	0.0110477
	Best	0.3995004	0.399306	0.3996816	0.3987943
	Worst	0.4410052	0.4491349	0.4557192	0.4428635
	Median	0.4106485	0.406472	0.4076855	0.4105367
F18	Index	17	7	18	18
	Mean	9.3000012	11.10058	8.4005383	7.5000008
	SD	11.614945	12.584091	10.984358	10.234325
	Best	3	3	3	3
	Worst	30.000013	30.00002	30.000011	30.000011
	Median	3	3	3	3
F19	Index	18	4	3	8
	Mean	− 3.8505681	− 3.8508949	− 3.8518311	− 3.852858
	SD	0.00588	0.0035879	0.0042009	0.0047404
	Best	− 3.8578257	− 3.857879	− 3.8603253	− 3.8611905
	Worst	− 3.8298316	− 3.8425129	− 3.8392971	− 3.8363528
	Median	− 3.8516327	− 3.8517318	− 3.8525449	− 3.8536414
F20	Index	5	7	5	12
	Mean	− 3.0410618	− 3.1018361	− 3.0709558	− 3.0730514
	SD	0.0921201	0.0778961	0.1056266	0.0945628
	Best	− 3.2350461	− 3.2494744	− 3.2261268	− 3.2513409
	Worst	− 2.8634044	− 2.8980305	− 2.7724918	− 2.8489681
	Median	− 3.0583833	− 3.1123699	− 3.1060803	− 3.099351
F21	Index	6	18	5	30
	Mean	− 3.7479617	− 4.2588219	− 3.5079814	− 3.8342777
	SD	1.3800636	1.5273327	1.15973	1.1648219
	Best	− 8.6037115	− 8.9291233	− 6.3095192	− 6.3553686
	Worst	− 1.794827	− 2.0148458	− 1.390897	− 1.7697845
	Median	− 3.5545286	− 3.834521	− 3.3704116	− 3.5955415

Table 15 (continued)

Function no	Parameters	Objective fitness function (10 dimensions)	Objective fitness function (30 dimensions)	Objective fitness function (50 dimensions)	Objective fitness function (100 dimensions)
F22	Index	13	30	14	21
	Mean	− 3.5086423	− 3.8007127	− 3.5578506	− 3.5019407
	SD	1.4662792	1.4745621	1.1441033	1.1145269
	Best	− 6.8760262	− 8.0583388	− 6.6029679	− 5.1052682
	Worst	− 1.3918829	− 1.4536972	− 1.7277629	− 1.601393
	Median	− 3.5870892	− 3.7268609	− 3.5793141	− 3.6208009
F23	Index	26	12	10	11
	Mean	− 4.1656536	− 4.5412382	− 3.6650576	− 3.8132129
	SD	1.6904521	1.6560109	1.8260066	1.6634419
	Best	− 8.212587	− 8.761818	− 8.5834305	− 8.2305609
	Worst	− 1.6650987	− 2.0013184	− 1.3407726	− 1.3802065
	Median	− 3.9062129	− 4.2167482	− 3.5149493	− 3.7151855

position are updated by employing Eqs. 16 and 17, respectively.

2.6.5 Stopping Criteria

If the maximum number of iterations is completed, the algorithm stops and G_{best} is considered as the optimal solution. Otherwise, steps 2.6.2 and 2.6.4 are repeated.

2.7 Database for Techno-Economic Evaluation

The techno-economic database required as input to optimize the size and operation of the proposed system is detailed as:

2.7.1 Electrical Load Requirements (kW)

The hourly load demand in the study area throughout the summer, moderate and winter seasons is demonstrated in Fig. 1. The maximum load demand for the study area is estimated in the summer, winter and moderate seasons as 177.71 kW, 177.71 kW and 182.12 kW, respectively.

2.7.2 Average Solar Irradiance (kWh/m.^{2}/day)

For the selected area, the availability of monthly average solar energy is depicted in Fig. 2. It is found to be highest in the month of May (7.08 kWh/m^2/day) and lowest in December (3.23 kWh/m^2/day) (NASA 2020).

2.7.3 Mean Air Temperature (°C)

The air temperature for different months of the year at the proposed location is presented in Fig. 3. It has been observed that the ambient temperature of the research area lies in the range of 8 °C–42 °C during the year.

2.7.4 Scheduling of Biogas and Biomass Generators

Bio-generators have been scheduled for operation when the load reaches the peak value for the proposed research area and are demonstrated in Table 3.

2.7.5 IHS and PSO Algorithm Parameters

For optimizing the objective function, various IHS algorithm parameters are detailed as: itr_{mx} = 150; HMR = 0.95; PR = 0.1; HMS = 5; PR_{mx} = 1; PR_{mn} = 0.1. The following parameters are set for the PSO algorithm: m = 4, C_1 = 2, C_2 = 2, S_p = 30, and i_{max} = 150.

2.7.6 Economical database of Hybrid System Components

The economic database of particular components of the hybrid system is listed in Table 4.

2.7.7 Project Parameters

In present research, the life of the system is 25 years with an 11% interest rate.

3 Result and Discussion

A concerted effort has been made to achieve the optimal size and design of the hybrid system made up of renewable energy resources. Firstly, under the off-grid mode, the three

Table 16 Quartile result for FD test function using IHS (10, 30, 50, 100 dimensions)

Dimension	Function no	No. of trials	Minimum value	Maximum value	Mean value	Median	First quartile (25th percentile)	Second quartile (50th percentile)	Third quartile (75th percentile)	Semi interquartile deviation	Number of outliers	SD
10 Dimensions	F14	30	0.9980038	12.670506	8.9586192	11.7187	2.9821052	11.7187	12.670506	4.8442003	0	4.688551
	F15	30	0.0003475	0.1207472	0.0160376	0.0019117	0.0003979	0.0019117	0.0122676	0.0059349	5	0.030964
	F16	30	− 1.031628	− 1.031628	− 1.031628	− 1.031628	− 1.031628	− 1.031628	− 1.031628	8.739E-08	0	1.339E-07
	F17	30	0.3995004	0.4410052	0.4123419	0.4106485	0.4048042	0.4106485	0.417018	0.0061069	0	0.0098248
	F18	30	3	30.000013	9.3000012	3	3	3	3.0000001	3.897E-08	7	11.614945
	F19	30	− 3.857826	− 3.829832	− 3.850568	− 3.851633	− 3.854023	− 3.851633	− 3.849013	0.0025053	2	0.0058799
	F20	30	− 3.235046	− 2.863404	− 3.041062	− 3.058383	− 3.100055	− 3.058383	− 2.964197	0.0679291	0	0.0921201
	F21	30	− 8.603711	− 1.794827	− 3.747962	− 3.554529	− 4.797739	− 3.554529	− 2.866853	0.965443	0	1.3800636
	F22	30	− 6.876026	− 1.391883	− 3.508642	− 3.587089	− 4.355181	− 3.587089	− 2.004937	1.175122	0	1.4662792
	F23	30	− 8.212587	− 1.665099	− 4.165654	− 3.906213	− 4.886637	− 3.906213	− 2.953976	0.9663309	0	1.6904521
30 Dimensions	F14	30	1.992031	12.67051	9.295883	10.76318	6.903336	10.76318	12.67051	2.883585	0	3.708035
	F15	30	0.000348	0.116226	0.016901	0.001071	0.000425	0.001071	0.017472	0.008523	3	0.03273
	F16	30	− 1.03163	− 1.03163	− 1.03163	− 1.03163	− 1.03163	− 1.03163	− 1.03163	8.13E-08	0	1.15E-07
	F17	30	0.399306	0.449135	0.409765	0.406472	0.402304	0.406472	0.413105	0.0054	1	0.010759
	F18	30	3	30.00002	11.10058	3	3	3	30	13.5	0	12.58409
	F19	30	− 3.85788	− 3.84251	− 3.85089	− 3.85173	− 3.85303	− 3.85173	− 3.84802	0.002508	0	0.003588
	F20	30	− 3.24947	− 2.89803	− 3.10184	− 3.11237	− 3.15205	− 3.11237	− 3.07989	0.036081	1	0.077896
	F21	30	− 8.92912	− 2.01485	− 4.25882	− 3.83452	− 4.97619	− 3.83452	− 3.13408	0.921058	0	1.527333
	F22	30	− 8.05834	− 1.4537	− 3.80071	− 3.72686	− 4.59725	− 3.72686	− 2.93309	0.83208	0	1.474562
	F23	30	− 8.76182	− 2.00132	− 4.54124	− 4.21675	− 5.98771	− 4.21675	− 3.29856	1.344571	0	1.656011
50 Dimensions	F14	30	0.998004	12.67051	9.550234	10.76318	7.873993	10.76318	12.67051	2.398256	0	3.870795
	F15	30	0.000353	0.108918	0.018105	0.004306	0.000392	0.004306	0.020357	0.009983	4	0.031536
	F16	30	− 1.03163	− 1.03163	− 1.03163	− 1.03163	− 1.03163	− 1.03163	− 1.03163	8.03E-08	1	1.75E-07
	F17	30	0.399682	0.455719	0.413056	0.407686	0.402741	0.407686	0.42037	0.008814	1	0.013823
	F18	30	3	30.00001	8.400538	3	3	3	3.001781	0.00089	7	10.98436
	F19	30	− 3.86033	− 3.8393	− 3.85183	− 3.85254	− 3.85402	− 3.85254	− 3.85011	0.001955	1	0.004201
	F20	30	− 3.22613	− 2.77249	− 3.07096	− 3.10608	− 3.12942	− 3.10608	− 3.01441	0.057504	1	0.105627
	F21	30	− 6.30952	− 1.3909	− 3.50798	− 3.37041	− 4.48799	− 3.37041	− 2.77835	0.854822	0	1.15973
	F22	30	− 6.60297	− 1.72776	− 3.55785	− 3.57931	− 4.04615	− 3.57931	− 2.77205	0.637052	0	1.144103
	F23	30	− 8.58343	− 1.34077	− 3.66506	− 3.51495	− 4.75072	− 3.51495	− 2.08499	1.332866	0	1.826007

Table 16 (continued)

Dimension	Function no	No. of trials	Minimum value	Maximum value	Mean value	Median	First quartile (25th percentile)	Second quartile (50th percentile)	Third quartile (75th percentile)	Semi interquartile deviation	Number of outliers	SD
100 Dimensions	F14	30	0.998004	12.67051	10.44458	12.67051	10.76318	12.67051	12.67051	0.953663	5	4.000326
	F15	30	0.000356	0.104987	0.020974	0.005446	0.000724	0.005446	0.023358	0.011317	4	0.031331
	F16	30	− 1.03163	− 1.03163	− 1.03163	− 1.03163	− 1.03163	− 1.03163	− 1.03163	8.38E-08	0	1.15E-07
	F17	30	0.398794	0.442864	0.412769	0.410537	0.404284	0.410537	0.419541	0.007629	0	0.011048
	F18	30	3	30.00001	7.500001	3	3	3	3	1.34E-08	5	10.23433
	F19	30	− 3.86119	− 3.83635	− 3.85286	− 3.85364	− 3.85535	− 3.85364	− 3.8497	0.002825	1	0.00474
	F20	30	− 3.25134	− 2.84897	− 3.07305	− 3.09935	− 3.13617	− 3.09935	− 3.03319	0.051492	0	0.094563
	F21	30	− 6.35537	− 1.76978	− 3.83428	− 3.59554	− 4.59042	− 3.59554	− 2.91296	0.838729	0	1.164822
	F22	30	− 5.10527	− 1.60139	− 3.50194	− 3.6208	− 4.54337	− 3.6208	− 2.49375	1.024811	0	1.114527
	F23	30	− 8.23056	− 1.38021	− 3.81321	− 3.71519	− 4.34758	− 3.71519	− 2.65391	0.846836	0	1.663442

models of renewable energy-based systems are considered in the present study, as elaborated below:

(a) Model M_{11}: SPV/Biomass/Battery
(b) Model M_{12}: SPV/Biogas/Battery
(c) Model M_{13}: SPV/Biomass/Biogas/Battery

The hourly simulations for each model have been conducted in MATLAB for one year. The parameters were optimized with the goal of minimizing the system's NPC, which was achieved by employing the IHS and PSO algorithms. The SPV/biomass/biogas/battery model connected to a grid has also been simulated on an hourly basis using both algorithms to validate the results. Finally, the results from off-grid models are compared with the grid-connected hybrid model, and the optimal option has been found.

The selected off-grid models are simulated for fulfilling the load demand of the proposed location on an hourly basis using IHS and PSO algorithms by simulating in MATLAB. The obtained result after hourly simulation along with the optimum size of each component is shown in Table 5.

It is observed that the most optimal off-grid model M_{11} comprises a 229.13 kW (975 nos.) SPV system, a 166 kW biomass gasifier system, and 544.8 kWh (227 nos.) of battery bank storage system along with a 100 kW converter. The optimum NPC of the model is calculated as \$7.17 * 10^5 and a CoE of \$0.105/kWh. It has also been reported that IHS gives more promising results compared to PSO.

3.1 Optimization Results of Grid-Integrated Hybrid Model

The optimization of the grid-integrated hybrid model, which consists of SPV/Biogas/Biomass/battery using IHS and PSO algorithms, was carried out, and the results are presented in Table 6.

It is concluded that the IHS model has given more accurate results as compared to the PSO algorithm. The optimal size of the grid-connected model obtained by the IHS algorithm is a 226.31 kW SPV array, a 41 kW biomass system, a 98 kW biogas system, a 55.2 kWh battery bank storage, and a 100 kW converter, with NPC and CoE calculated as \$6.00 * 10^5 and \$0.081/kWh, respectively.

3.2 Comparative Analysis of Off-Grid and Grid-Connected Models

The grid-integrated model is compared with off-grid models in terms of NPC and CoE. Tables 5 and 6 reveal that the grid-integrated model has a lower value for NPC and CoE than the off-grid models. Besides, it is also

Table 17 Test result of FD benchmark functions using IHS algorithm for 10, 30, 50 and 100 dimensions

Function no	Parameters		Objective fitness function (10 dimensions)	Objective fitness function (30 dimensions)	Objective fitness function (50 dimensions)	Objective fitness function (100 dimensions)
F14	Wilcoxon rank sum test	p-rank	1	0.0962628	0.935192	0.3790363
		h-rank	0	0	0	0
	T-test	p-test	0	0	0	0
		t-test	0.8832565	0.1528692	0.8789596	0.8548552
F15	Wilcoxon rank sum test	p-rank	0.3041768	0.491783	0.6520436	0.2972717
		h-rank	0	0	0	0
	T-test	p-test	0	0	0	0
		t-test	0.7973219	0.8082163	0.0736713	0.6062152
F16	Wilcoxon rank sum test	p-rank	0.2115612	0.7618283	0.9705161	0.7171888
		h-rank	0	0	0	0
	T-test	p-test	0	0	0	0
		t-test	0.3501874	0.7894639	0.967972	0.8030388
F17	Wilcoxon rank sum test	p-rank	0.5395103	0.2643262	0.7282653	0.8187457
		h-rank	0	0	0	0
	T-test	p-test	0	0	0	0
		t-test	0.5242866	0.8078773	0.8046798	0.4345065
F18	Wilcoxon rank sum test	p-rank	0.6952154	0.17145	0.935192	0.1153624
		h-rank	0	0	0	0
	T-test	p-test	0	0	0	0
		t-test	0.7864796	0.1694317	0.5362894	0.1607109
F19	Wilcoxon rank sum test	p-rank	0.7958455	0.5105979	0.2707053	0.2707053
		h-rank	0	0	0	0
	T-test	p-test	0	0	0	0
		t-test	0.790141	0.4404338	0.1883748	0.3970414
F20	Wilcoxon rank sum test	p-rank	0.1259702	0.2225729	0.0992576	0.7505872
		h-rank	0	0	0	0
	T-test	p-test	0	0	0	0
		t-test	0.1609095	0.2516846	0.1547637	0.9142226
F21	Wilcoxon rank sum test	p-rank	0.7171888	0.2707053	0.0191124	0.8766349
		h-rank	0	0	1	0
	T-test	p-test	0	0	1	0
		t-test	0.5228637	0.2268478	0.0099076	0.8635955

Table 17 (continued)

Function no	Parameters		Objective fitness function (10 dimensions)	Objective fitness function (30 dimensions)	Objective fitness function (50 dimensions)	Objective fitness function (100 dimensions)
F22	Wilcoxon rank sum test	*p*-rank	0.2009489	0.8766349	0.7393988	0.0962628
		h-rank	0	0	0	0
	T-test	*p*-test	0	0	0	0
		t-test	0.1387403	0.8241737	0.8465256	0.0825139
F23	Wilcoxon rank sum test	*p*-rank	0.0701266	0.074827	0.3870998	0.3183042
		h-rank	0	0	0	0
	T-test	*p*-test	1	1	0	0
		t-test	0.0415531	0.0118357	0.5656017	0.3863183

observed that the grid-connected model has the lowest battery storage capacity of 55.2 kWh to meet the full load demand. As a result, the grid-connected model is better and is proposed for the selected area given economic concerns. Further, the results of different parameters of the proposed model are presented in the forthcoming sections.

3.3 IHS and PSO Algorithm Convergence Curve for Proposed Model

The convergence curve for the IHS and the PSO algorithm of the proposed grid-connected model is shown in Fig. 4.

From Fig. 4, it is observed that IHS converges completely and provides a fixed value at the 128th iteration. However, PSO has converged to a constant value after the 140th iteration. Therefore, it is obvious that IHS has a faster convergence than PSO. Besides, to test the efficacy of the proposed IHS optimization model, a set of different benchmark functions is considered, which comprises three major benchmark feature classes: Uni Modal (UM) benchmark functions F1, F2, F3, F4, F5, F6 and F7; Multi-Modal (MM) benchmark functions F8, F9, F10, F11, F12, and F13; and benchmark problems of Fixed Dimensions (FD) are considered (Bhattacharya et al. 2021; Dhawale et al. 2021). The values of the mean, standard deviation (SD), best value, worst value, median, quartile, Wilcoxon sum test, statistical *T* test, and simulation time result are computed for each of the objective functions for 10, 30, 50, and 100 dimensions, respectively, and demonstrated in Tables 7, 8, 9, 10, 11, 12, 13, 14, 15, 16, 17 and 18. In the present work, 30 trial runs are considered, and the proposed model is simulated for a maximum of 500 iterations. The proposed optimization model was tested at 2.60 GHz on Intel ® Core TM and i7-5600 CPUs.

3.4 Annual Energy Generation by Grid-Connected Optimal Model

The contribution of different renewable energy resources to the annual generation of electricity by the proposed grid-connected model is shown in Fig. 5.

The obtained result clearly shows that the SPV array produced the maximum amount of electricity of 450,570 kWh/year (65.56%), followed by biomass with 182,885 kWh/year (26.61%) and biogas with 53,822 kWh/year (7.83%).

3.5 Cost-wise Breakup of NPC

The proportion of the cost breakup in the overall NPC of the proposed model is given in Table 19. The cost of grid purchase was found to have the highest share of $280,400 among all costs.

3.6 Component-wise Breakup of NPC

The contribution of different system components is shown in Fig. 6. Biomass has been observed to have the biggest part of a total of 50% of NPC, followed by biogas with 19%, the SPV panel with 14%, the battery with 11% and the converter with 6%.

Table 18 Simulation time of FD benchmark functions using IHS algorithm for 10, 30, 50 and 100 dimensions

Function no	Parameters	Objective fitness function (10 dimensions)	Objective fitness function (30 dimensions)	Objective fitness function (50 dimensions)	Objective fitness function (100 dimensions)
F14	Best time (Sec)	–	0.359375	0.34375	–
	Average time (Sec.)	–	0.3869792	0.384375	–
	Worst time (Sec)	–	0.46875	0.4375	–
F15	Best time (Sec)	0.03125	0.03125	0.03125	0.03125
	Average time (Sec.)	0.0536458	0.0411458	0.0583333	0.0510417
	Worst time (Sec)	0.09375	0.09375	0.109375	0.09375
F16	Best time (Sec)	0.03125	0.03125	0.03125	0.03125
	Average time (Sec.)	0.0541667	0.0416667	0.0536458	0.0526042
	Worst time (Sec)	0.09375	0.078125	0.125	0.078125
F17	Best time (Sec)	0.03125	0.03125	0.015625	0.015625
	Average time (Sec.)	0.0776042	0.0541667	0.0661458	0.0609375
	Worst time (Sec)	0.171875	0.1875	0.171875	0.171875
F18	Best time (Sec)	0.015625	0.015625	0.03125	0.015625
	Average time (Sec.)	0.0489583	0.0307292	0.0473958	0.0442708
	Worst time (Sec)	0.078125	0.046875	0.0625	0.0625
F19	Best time (Sec)	0.03125	0.03125	0.03125	0.03125
	Average time (Sec.)	0.0640625	0.0473958	0.065625	0.0526042
	Worst time (Sec)	0.09375	0.09375	0.15625	0.09375
F20	Best time (Sec)	0.03125	0.03125	0.046875	0.03125
	Average time (Sec.)	0.0614583	0.05	0.0729167	0.0546875
	Worst time (Sec)	0.109375	0.0625	0.125	0.078125
F21	Best time (Sec)	0.046875	0.03125	0.03125	0.046875
	Average time (Sec.)	0.0697917	0.0640625	0.0739583	0.0682292
	Worst time (Sec)	0.109375	0.140625	0.109375	0.109375
F22	Best time (Sec)	0.0625	0.046875	0.0625	0.046875
	Average time (Sec.)	0.0796875	0.0703125	0.0875	0.0786458
	Worst time (Sec)	0.109375	0.109375	0.140625	0.09375

Table 18 (continued)

Function no	Parameters	Objective fitness function (10 dimensions)	Objective fitness function (30 dimensions)	Objective fitness function (50 dimensions)	Objective fitness function (100 dimensions)
F23	Best time (Sec)	0.0625	0.0625	0.0625	0.0625
	Average time (Sec.)	0.09375	0.08125	0.0994792	0.0796875
	Worst time (Sec)	0.171875	0.125	0.15625	0.171875

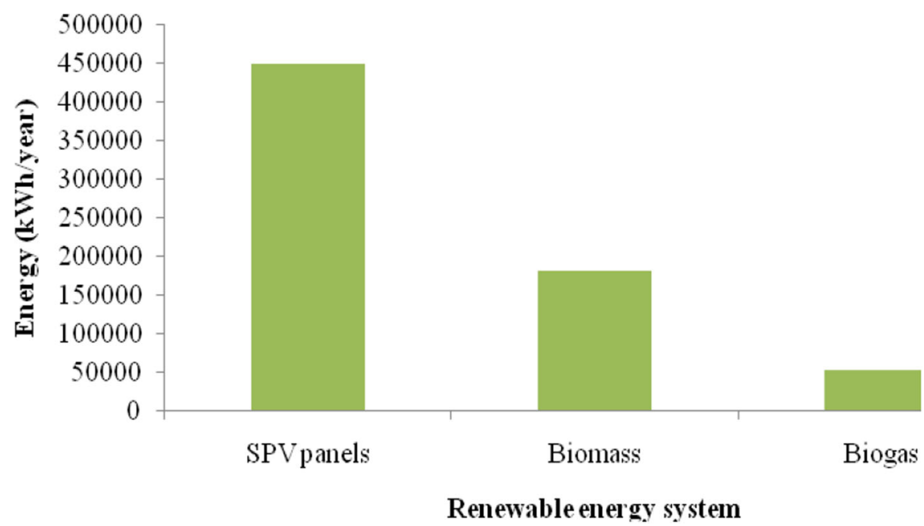

Fig. 5 Share of renewable energy resources in annual energy generation

Table 19 Cost-wise breakup of NPC

S. no	Indicator	Value ($)	Percentage (%)
1	Capital cost	143,665	21
2	O & M cost	128,260	19
3	Fuel cost	68,840	10
4	Salvage value	11,106	01
5	Revenue from grid sale	54,965	08
6	Cost of grid purchase	280,400	41

3.7 Seasonal Energy Sale and Purchase to/from Grid

Seasonal energy sold and purchased from the utility grid has been shown in Table 20. It is concluded that in the summer season, the proposed model buys more energy, followed by the moderate and winter seasons. It is due to the increased demand for energy during the summer. Furthermore, grid sales and grid purchases are relatively lower in the winter than in the summer and the moderate seasons due to lower energy demand.

4 Conclusion

In this research, the modeling and optimization of the hybrid energy system based on renewable energy resources has been carried out in the remote area of Sonipat, India. Based on the available renewable energy resources, different configurations for off-grid and grid-connected scenarios are developed and presented. From the developed configurations, an optimized model is selected to electrify the given location based on NPC and CoE. The IHS, a newly developed algorithm, and PSO algorithms have been used to optimize the hybrid energy system.

The size optimization of the hybrid renewable energy system for the grid-connected scenario is obtained as a 226.31 kW SPV array, 98 kW biogas system, 41 kW biomass system, 100 kW converter, and 55.2 kWh of battery bank storage. The total NPC and CoE are estimated to be $\$6.00 * 10^5$ and \$0.081/kWh, respectively. The findings of the study may be used to develop a hybrid renewable energy system for other related areas having the same geographical parameters.

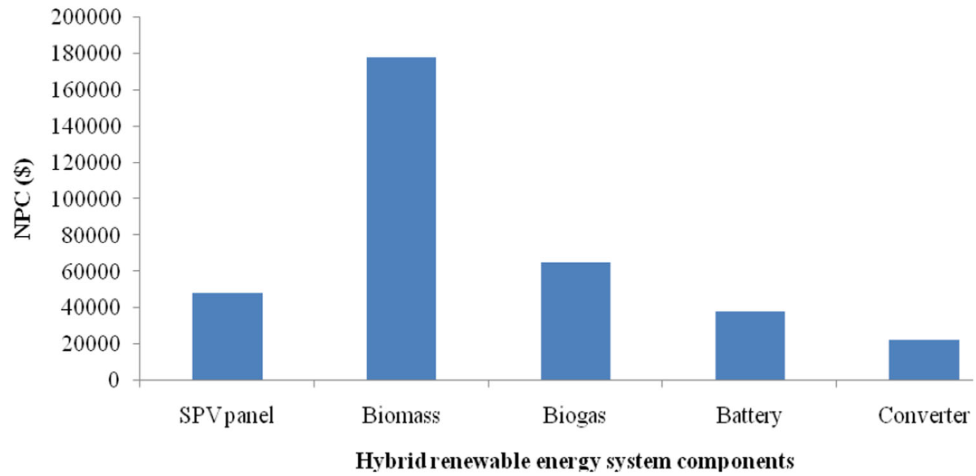

Fig. 6 Share of different renewable energy resources in NPC

Table 20 Seasonal sale and purchase of energy to grid

Season	Grid sale energy (kWh)	Grid purchase energy (kWh)
Summer season	17,244	133,720
Moderate season	15,790	76,482
Winter season	19,263	36,065
Total (kWh/year)	52,297	246,260

References

Alaaeldin M, Abdelshafya HH, Jakub J (2018) Optimal design of a grid-connected desalination plant powered by renewable energy resources using a hybrid PSO-GWO approach. Energy Convers Manage 173:331–347

Alturki FA, Abdullrahman A, Al-Shamma'a AA, Farh HMH, AlSharabi K (2020) Optimal sizing of autonomous hybrid energy system using supply-demand-based optimization algorithm. Int J Energy Res 2020:1–21

Anand P, Bath SK, Rizwan M (2017) Design and development of stand-alone renewable energy-based hybrid power system for remote base transceiver station. Int J Comput Appl 169:34–41

Anand P, Bath SK, Rizwan M (2019a) Renewable energy-based hybrid model for rural electrification. Int J Energy Technol Policy 15:86–113

Anand P, Rizwan M, Bath SK (2019b) Sizing of a renewable energy-based hybrid system for rural electrification using a grey wolf optimization approach. IET Energy Syst Integr 1:1–15

Anand P, Bath SK, Rizwan M (2020) Size Optimization of RES based grid-connected hybrid power system using a harmony search algorithm. Int J Energy Technol Policy 16:238–276

Arévaloa P, Benavidesa D, Lata-Garcíac J, Jurado F (2020) Energy control and size optimization of a hybrid system (photovoltaic-hidrokinetic) using various storage technologies. Sustain Cities Soc 52:1–17

Askarzadeh A (2013a) A discrete chaotic harmony search-based simulated annealing algorithm for optimum design of PV/Wind hybrid system. Sol Energy 97:93–101

Askarzadeh A (2013b) Developing a discrete harmony search algorithm for size optimization of the wind-photovoltaic hybrid energy system. Sol Energy 98:190–195

Askarzadeh A, dos Leandro SC (2015) A novel framework for optimization of a grid independent hybrid renewable energy system: a case study of iran. Sol Energy 112:383–396

Bartolucci L, Cordiner S, Mulone V, Rocco V, Rossi JL (2018) Hybrid renewable energy systems for renewable integration in microgrids: influence of sizing on performance. Energy 152:744–758

Bhattacharya S, Tripathi SL, Kamboj VK (2021) Design of tunnel FET architectures for low power application using improved Chimp optimizer algorithm. Eng Comput. https://doi.org/10.1007/s00366-021-01530-4

Borowy BS, Salameh ZM (1996) Methodology for optimally sizing the combination of a battery bank and PV array in a wind/ PV hybrid system. IEEE Trans Energy Convers 11:367–375

Chauhan A, Saini RP (2015) Renewable energy-based off-grid rural electrification in uttarakhand state of india: technology options, modeling method, barriers and recommendations. Renew Sustain Energy Rev 51:662–681

Chauhan A, Saini RP (2016) Discrete harmony search based size optimization of integrated renewable energy system for remote rural areas of Uttarakhand state in India. Renewable Energy 94:587–604

Chauhan A, Saini RP (2017) Size optimization and demand response of a stand-alone integrated renewable energy system. Energy 124:59–73

Das BK, Hasan M (2021) Optimal sizing of a stand-alone hybrid system for electric and thermal loads using excess energy and waste heat. Energy 214:119036

Delnia S, Naghshbandy AH, Bahramara S (2020) Optimal sizing of hybrid renewable energy systems in presence of electric vehicles using multi-objective particle swarm optimization. Energy 209:1–17

Dey B, Bhattacharyya B, Sharma S (2019) Optimal sizing of distributed energy resources in a microgrid system with highly penetrated renewables. Iran J Sci Technol Trans Electr Eng 43:527–540

Dhawale D, Kamboj VK, Anand P (2021) An effective solution to numerical and multi-disciplinary design optimization problems using chaotic slime mold algorithm. Eng Comput. https://doi.org/10.1007/s00366-021-01409-4

Eteiba M, Barakat SH, Samy MM, Wahba WI (2018) Optimization of an off-grid pv/biomass hybrid system with different battery technologies. Sustain Cities Soc 40:713–727

Ghaffari A, Askarzadeh A (2020) Design optimization of a hybrid system subject to reliability level and renewable energy penetration. Energy 193:116754

Kamboj V, Bath SK, Dhillon JS (2016) Implementation of hybrid harmony search/random search algorithm for single area unit commitment problem. Electr Power Energy Syst 77:228–249

Karaki S, Chedid R, Ramadan R (1999) Probabilistic performance assessment of autonomous solar-wind energy conversion systems. IEEE Trans Energy Convers 14:766–772

Li J, Wei W, Xiang J (2012) A simple sizing algorithm for stand-alone pv/wind/battery hybrid microgrids. Energies 5:5307–5323

Li D, Zhu D, Wang R, Ge M, Wu S, Cai Y (2020) Sizing optimization and experimental verification of a hybrid generation water pumping system in a greenhouse. Math Probl Eng 2020:1–11

Lu X, Wang H (2020) Optimal sizing and energy management for cost-effective PEV hybrid energy storage systems. IEEE Trans Ind Inform 6:3407–3416

Lujano-Rojas JM, Dufo-López R, Bernal-Agustín JL (2013) Probabilistic modelling and analysis of stand-alone hybrid power systems. Energy 63:19–27

Mahesh A, Sandhu KS (2019) Optimal sizing of a grid-connected PV/Wind/Battery system using particle swarm optimization. Iran J Sci Technol Trans Electr Eng 43:107–121

Markvart T, Fragaki A, Ross J (2006) PV system sizing using observed time series of solar radiation. Sol Energy 80:46–50

Ministry of new and renewable energy (2020) Government of India, www.mnre.gov.in Accessed 10 April 2020

Mubaarak S, Zhang D, Wang L, Mohan M, Kumar PM, Li C, Zhang Y, Li M (2021) Efficient photovoltaics-integrated hydrogen fuel cell-based hybrid system: energy management and optimal configuration. Renew Sustain Energy 13:1–12

Paliwal P, Patidar NP, Nema RK (2014) Determination of reliability constrained optimal resource mix for an autonomous hybrid power system using particle swarm optimization. Renew Energy 63:194–204

Singh S, Singh M, Kaushik SC (2016) Optimal sizing of grid integrated hybrid PV-biomass energy system using artificial bee colony algorithm. IET Renew Power Gener 10:642–650

Solar Irradiance and Air temperature of study area: NASA (2020) Surface meteorology and solar energy: a renewable energy resource. https://eosweb.larc.nasa.gov/sse/ Accessed on 19 May 2020

Sufyan M, Abd Rahim N, Tan C, Muhammad A, Sheikh Raihan SR (2019) Optimal sizing and energy scheduling of isolated microgrid considering the battery lifetime degradation. PLoS ONE 14:1–28

Wu T, Zhang H, Shang L (2020) Optimal sizing of a grid-connected hybrid renewable energy systems considering hydroelectric storage. Energy Sour Part A Recovery Utili Environ Eff 2020:1–17

Zebarjadi M, Askarzadeh A (2016) Optimization of a reliable grid-connected PV-based power plant with/without energy storage system by a heuristic approach. Sol Energy 125:12–21

Zhang X, Tan SC, Li G, Li J, Fang Z (2013) Components sizing of hybrid energy systems via the optimization of power dispatch simulations. Energy 52:165–172